Curvature thylakoid 1 proteins modulate prolamellar body morphology and promote organized thylakoid biogenesis in *Arabidopsis thaliana*

Omar Sandoval-Ibáñez[a,b,1], Anurag Sharma[a,1], Michał Bykowski[c,1], Guillem Borràs-Gas[a], James B. Y. H. Behrendorff[a], Silas Mellor[a], Klaus Qvortrup[d], Julian C. Verdonk[e], Ralph Bock[b], Łucja Kowalewska[c,2], and Mathias Pribil[a,2]

[a]Copenhagen Plant Science Centre, Department of Plant and Environmental Sciences, University of Copenhagen, 1871 Copenhagen, Denmark; [b]Max Planck Institute of Molecular Plant Physiology, Department of Organelle Biology, Biotechnology and Molecular Ecophysiology, 14476 Potsdam, Germany; [c]Department of Plant Anatomy and Cytology, Institute of Experimental Plant Biology and Biotechnology, Faculty of Biology, University of Warsaw, PL-02-096 Warsaw, Poland; [d]Core Facility for Integrated Microscopy, The Panum Institute, Department of Biomedical Sciences, University of Copenhagen, 2200 Copenhagen, Denmark; and [e]Horticulture and Product Physiology, Plant Sciences Group, Wageningen University, 6708 PD Wageningen, The Netherlands

Edited by Krishna K. Niyogi, University of California, Berkeley, CA, and approved August 24, 2021 (received for review August 5, 2021)

The term "de-etiolation" refers to the light-dependent differentiation of etioplasts to chloroplasts in angiosperms. The underlying process involves reorganization of prolamellar bodies (PLBs) and prothylakoids into thylakoids, with concurrent changes in protein, lipid, and pigment composition, which together lead to the assembly of active photosynthetic complexes. Despite the highly conserved structure of PLBs among land plants, the processes that mediate PLB maintenance and their disassembly during de-etiolation are poorly understood. Among chloroplast thylakoid membrane–localized proteins, to date, only Curvature thylakoid 1 (CURT1) proteins were shown to exhibit intrinsic membrane-bending capacity. Here, we show that CURT1 proteins, which play a critical role in grana margin architecture and thylakoid plasticity, also participate in de-etiolation and modulate PLB geometry and density. Lack of CURT1 proteins severely perturbs PLB organization and vesicle fusion, leading to reduced accumulation of the light-dependent enzyme protochlorophyllide oxidoreductase (LPOR) and a delay in the onset of photosynthesis. In contrast, overexpression of CURT1A induces excessive bending of PLB membranes, which upon illumination show retarded disassembly and concomitant overaccumulation of LPOR, though without affecting greening or the establishment of photosynthesis. We conclude that CURT1 proteins contribute to the maintenance of the paracrystalline PLB morphology and are necessary for efficient and organized thylakoid membrane maturation during de-etiolation.

CURT1 | de-etiolation | prolamellar bodies | chloroplast biogenesis | photosynthesis

The transition from etioplast to chloroplast is a highly dynamic process involving changes in membrane structure accompanied by reprogramming of nuclear and plastid gene expression as well as metabolism (1–3). Etioplasts contain an internal network of paracrystalline membranes known as prolamellar bodies (PLBs), from which porous prothylakoid (PT) membranes protrude (4). Recent studies using advanced electron tomography (ET) have elucidated the structural rearrangements in PLBs and PTs during de-etiolation (5). These investigations have shown that upon illumination, the regularity of the paracrystalline network of PLBs progressively declines, while PTs elongate from the margins of PLBs, forming parallel rows oriented along one axis of the etio-chloroplast. Over time, PTs undergo further morphological changes, which transform porous and discontinuous membranes into flat, layered lamellae—the first grana stacks (5). During this process, the protein and pigment content of the PTs changes drastically. Etioplasts contain not only high concentrations of ATPase precomplexes, ferredoxin-$NADP^+$ oxidoreductase, and FtsH and Clp proteases (6) but also several glycolytic enzymes, including enolase and phosphoglyceromutase, and phosphoenolpyruvate translocators (7). Moreover, the PLBs in etioplasts accumulate copious amounts of the light-dependent enzyme NADPH:protochlorophyllide oxidoreductase (LPOR) and the precursor pigment protochlorophyllide (Pchlide), which together form a photoactivatable complex (1, 4, 6, 8). Upon illumination, LPOR-containing complexes drive the conversion of Pchlide to chlorophyllide and rapidly disintegrate, with the concomitant degradation of LPOR. The subsequent conversion of chlorophyllide into chlorophyll by downstream tetrapyrrole pathway enzymes is accompanied by the synthesis of chlorophyll-binding proteins, such as the light-harvesting complexes (LHCs) and PSI and PSII core proteins (4, 9, 10), and leads to the de novo assembly and organization of photosynthetic complexes in the thylakoid membranes (1, 11–13).

Various mutants that are defective in thylakoid development have been characterized. The genes affected code for assembly factors (e.g., *sco2* and *hcf222*) (14, 15), enzymes of lipid biosynthesis

Significance

Chloroplast biogenesis is a fundamental process occurring during seedling ontogenesis and leading to plant autotrophy. Which membrane components sterically organize the light-triggered transition of etioplast prolamellar bodies (PLBs) into chloroplast thylakoids, and thus mediate cubic–lamellar transformation, is poorly understood. Here, we used combined two- and three-dimensional electron microscopy, spectroscopy, and biochemical methods to determine the role of CURT1 proteins in the formation of etioplast cubic membranes and their transformation to photosynthetically active chloroplast thylakoids. CURT1 proteins were previously recognized as significant contributors to thylakoid membrane folding. We found that CURT1 proteins are integral proteins of etioplast membranes and act as factors modulating PLBs and prothylakoid nanomorphology. They are also required for concerted thylakoid maturation under de-etiolation.

Author contributions: O.S.-I., A.S., J.B.Y.H.B., S.M., R.B., Ł.K., and M.P. designed research; O.S.-I., A.S., M.B., G.B.-G., J.B.Y.H.B., S.M., K.Q., J.C.V., and Ł.K. performed research; K.Q. contributed new reagents/analytic tools; O.S.-I., A.S., M.B., G.B.-G., J.C.V., Ł.K., and M.P. analyzed data; and O.S.-I., R.B., Ł.K., and M.P. wrote the paper.

The authors declare no competing interest.

This article is a PNAS Direct Submission.

[1]O.S.-I., A.S., and M.B. contributed equally to this work.

[2]To whom correspondence may be addressed. Email: pribil@plen.ku.dk or lucja.kowalewska@uw.edu.pl.

This article contains supporting information online at https://www.pnas.org/lookup/suppl/doi:10.1073/pnas.2113934118/-/DCSupplemental.

Published October 15, 2021.

(*mgd1* and *dgd1*) (16, 17), and transcription factors (including the ABI4-HY5 cascade and OR-TCP14) (18, 19) among other functions. Their phenotypes range from mild defects in thylakoid biogenesis (i.e., mutants of the OR-TCP14 pathway) to severe effects in PLB and PT ultrastructure or plant death (e.g., lipid mutants). Indeed, only the use of DEX-inducible amiRNA-*dgd1* and amir-RNA-*mdg1* lines made it possible to explore the roles of monogalactosyldiacylglycerol (MGDG) synthetase 1 (MGD1) and diacylgalactosyldiacylglycerol synthase 1 (DGD1), respectively, in lipid bilayer formation during thylakoid biogenesis (20). These studies have contributed significantly to our understanding of PLB biogenesis, especially the morphological impact of lipids, pigments, and photosynthesis-related proteins on this process. However, the components that mediate the morphological transformation of PLBs remain elusive, although the available evidence argues for participation of membrane-bending proteins (5).

Curvature Thylakoid 1 (CURT1) proteins are major contributors to the shaping of chloroplast thylakoid membranes (21). In *Arabidopsis thaliana,* they comprise a family of four thylakoid membrane-anchored proteins—named CURT1A to D—with molecular weights ranging between 11 and 15 kDa. CURT1A, the major isoform, induces thylakoid bending both in vitro and in planta (21). In the *A. thaliana curt1abcd* quadruple mutant (lacking all four CURT1 proteins), the grana diameter is increased, while the efficiency of light acclimation mechanisms such as state transitions and the PSII repair cycle (22) is impaired. The former effect can be expected to diminish the efficiency of plastocyanin-mediated electron transport (due to the

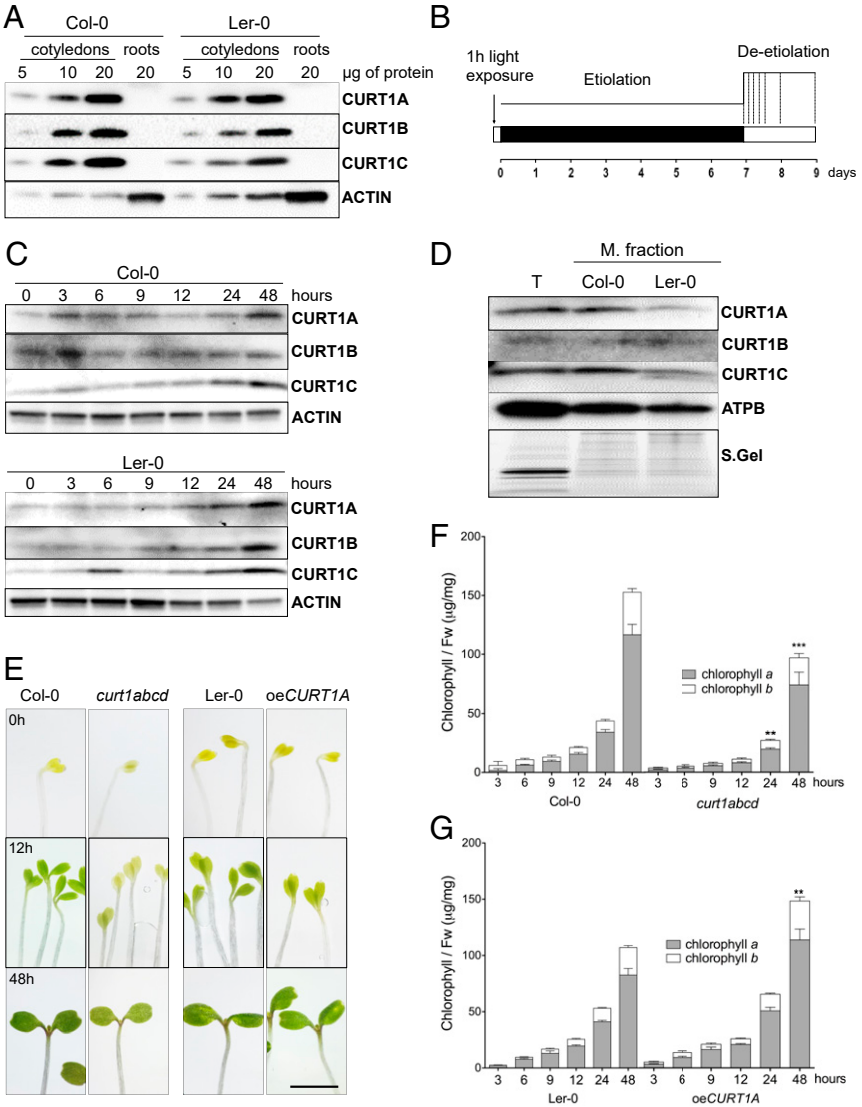

Fig. 1. CURT1 proteins are present in membrane fractions of cotyledons throughout de-etiolation. (*A*) Accumulation of CURT1A-C proteins in cotyledons and roots of 7-d-old Col-0 and Ler-0 seedlings grown under a 16/8 h light/dark cycle. ACTIN was used as the loading control. (*B*) Design of the de-etiolation assay. Seeds were stratified for 2 to 3 d and exposed to light for 1 h prior to dark acclimation for 1 wk. Seedlings were sampled at 0, 3, 6, 9, 12, 24, and 48 h after the onset of continuous light (dotted lines). (*C*) Immunoblotting analysis of CURT1A-C accumulation in total protein extracts from seedlings sampled at the times shown in *B*; 10 µg of protein was loaded in each lane. $n = 3$. (*D*) Membrane fractions (M. fractions) were prepared from cotyledons after 6 h of illumination. The accumulation of CURT1A-C proteins in mature thylakoids (T) and membrane fractions was analyzed in Col-0 and Ler-0. AtpB, a typical integral membrane protein, served as the loading control. $n = 3$. (*E*) Images of emerging cotyledons from Col-0, *curt1abcd*, Ler-0, and oe*CURT1A* at 0, 12, and 48 h after the onset of illumination. (Scale bar, 5 mm.) (*F* and *G*) Total chlorophyll content analyzed in (*F*) Col-0, *curt1abcd*, and (*G*) Ler-0 and oe*CURT1A* after 3, 6, 9, 12, 24, and 48 h of de-etiolation. The contributions of chlorophyll *a* (black columns) and chlorophyll *b* (white columns) to the total chlorophyll content are depicted. Error bars represent SDs of six biological replicates. Levels at 48 h were compared (by two-way ANOVA with Bonferroni posttest) between *curt1abcd* and Col-0 and between oe*CURT1A* and Ler-0. $^{**}P < 0.01$; $^{***}P < 0.001$.

longer distance covered by diffusion), which can in turn account for the latter phenotype (23). The cyanobacterial ortholog of CURT1A, *syn*CurT, has been postulated to play a role in both thylakoid morphology and thylakoid biogenesis (24), raising questions regarding the possible role of CURT1 proteins during thylakoid biogenesis in land plants. In the present work, we explore the impact of CURT1 proteins on PLB structure and membrane reorganization during the formation of a functional photosynthetic apparatus upon induction of de-etiolation in *A. thaliana* seedlings.

Results

CURT1s Are Membrane-Integral Etioplast Proteins that Affect Chlorophyll Accumulation during De-etiolation. To determine CURT1 protein profiles in seedlings, total protein extracts obtained from cotyledons and roots of 7-d-old seedlings were analyzed by immunoblotting (Fig. 1*A*). CURT1 proteins (CURT1A-C) were detected only in cotyledons but not in roots of the wild-type (WT) *A. thaliana* ecotypes Columbia-0 (Col-0) and Landsberg erecta-0 (Ler-0) (Fig. 1*A*). In agreement with previous studies (21), CURT1D was undetectable by immunoblotting. As CURT1 proteins were only detectable in cotyledons, we followed their accumulation during de-etiolation in more detail (Fig. 1*B*). We detected similar levels of CURT1A, B, and C in total protein fractions of etiolated and de-etiolated seedlings throughout the first 24 h of de-etiolation. Only after 48 h of illumination, an increase in CURT1 amounts was observed which correlated with the appearance of leaves primordial (Fig. 1*C*). We further detected CURT1 protein accumulation in membrane fractions of de-etiolated seedlings after 6 h of illumination (Fig. 1*D*). The presence of CURT1A and LPOR in the same membrane fraction after 15 min of illumination (*SI Appendix*, Fig. S1*A*), together with the concomitant decrease of LPOR after 6 h and 48 h of de-etiolation (*SI Appendix*, Fig. S1*B*), implies that CURT1 proteins are membrane localized within the etioplast.

For an extensive study of the roles of CURT1 proteins during greening, we made use of two previously characterized *A. thaliana* mutant lines: *curt1abcd*, which is devoid of all four CURT1 isoforms in the Col-0 background, and oe*CURT1A*, a CURT1A::c-Myc–tagged overexpressor line in the Ler-0 background which accumulates around 2.3 times more CURT1A protein in mature plants than the respective WT (21, 22). Both of these lines and their corresponding WT controls were subjected to the de-etiolation protocol (Fig. 1*B*). We observed that CURT1A accumulated around 30-fold in oe*CURT1A* compared to Ler-0 in etiolated tissue and that CURT1A levels altered only marginally during de-etiolation (*SI Appendix*, Fig. S1 *C* and *D*). In addition, we observed a delay in the greening of *curt1abcd* seedlings (relative to Col-0) at 12 h postillumination (Fig. 1*E* and *SI Appendix*, Fig. S2), consistent with reduced contents of total chlorophyll after 24 and 48 h of illumination (Fig. 1*F*). Although no notable differences in greening were observed between oe*CURT1A* and Ler-0 (Fig. 1*E* and *SI Appendix*, Fig. S2), a clear increase in total chlorophyll content in oe*CURT1A* compared to Ler-0 was detected after 48 h of illumination (Fig. 1*F*). Together, our results show that CURT1A, B, and C are membrane-associated proteins present in etio-chloroplasts and have an impact on chlorophyll accumulation during de-etiolation.

CURT1A-Mediated Changes in LPOR Degradation and Accumulation of Photosynthetic Proteins Correlate with the Modifications in PLB and PT Structures. To unravel the function of CURT1 proteins in the development of the photosynthetic apparatus during de-etiolation, we analyzed the accumulation of photosynthesis-related proteins in total protein extracts from seedlings of all four genotypes at different stages of de-etiolation. We observed that in *curt1abcd*, LPOR was present in lower amounts in etiolated seedlings, while it was more abundant in oe*CURT1A*, relative to the WT controls (Fig. 2*A*). Interestingly, the degradation of LPOR appeared to be delayed in oe*CURT1A*, while it was accelerated in *curt1abcd* (Fig. 2*A*). In agreement with previous studies (4), all four genotypes exhibited a rapid decline in *LPOR* transcript accumulation upon illumination. Lower *LPOR* messenger ribonucleic acid (mRNA) levels were observed in etiolated seedlings of *curt1abcd* (*SI Appendix*, Fig. S3), which partially explains the lower protein content observed in etiolated tissue but not the faster degradation of LPOR proteins. In contrast, *LPOR* transcript levels in oe*CURT1A* behaved similarly to those in Ler-0 (*SI Appendix*, Fig. S3), suggesting that protein degradation rather than LPOR transcription or mRNA stability is altered in oe*CURT1A*.

In *curt1abcd*, we observed a delay in the accumulation of PSII and PSI core proteins, including D1 (PsbA), D2 (PsbD), CP43 (PsbC), and PsaB. Their levels remain lower than in Col-0 throughout the course of de-etiolation (Fig. 2*A* and *SI Appendix*, Fig. S4). While *psbA* transcript levels were lower in *curt1abcd* (*SI Appendix*, Fig. S3), no differences in *psaA* transcripts were observed between *curt1abcd* and Col-0 (*SI Appendix*, Fig. S3). In contrast, no notable differences in PsaB, D1, or D2 protein concentrations were detectable between oe*CURT1A* and L*er*-0, in agreement with the *psaA* and *psbA* transcript levels in both genotypes (Fig. 2*A* and *SI Appendix*, Fig. S3). Notably, the amounts of CP43 were lower in oe*CURT1A* (*SI Appendix*, Fig. S4). Although a decrease in *LHCA1* transcripts was observed in *curt1abcd* after 24 h of illumination (*SI Appendix*, Fig. S4), levels of the Lhca1 protein were not notably affected (Fig. 2*A*). Amounts of both the PSII antenna protein Lhcb2 and its mRNA were altered in *curt1abcd* relative to Col-0 (Fig. 2*A* and *SI Appendix*, Fig. S3). In oe*CURT1A*, levels of Lhca1 exceeded those in Ler-0, while Lhcb2 amounts were lower (Fig. 2*A*). Consistent with previous studies (1, 6), no major changes in the accumulation of AtpB, RbcL, or PetA (cytochrome *f*) were detected in *curt1abcd* or oe*CURT1A* (Fig. 2*A* and *SI Appendix*, Fig. S4).

The delayed greening in *curt1abcd* together with the altered transcript and protein profiles observed in both *curt1abcd* and *oeCURT1A* prompted us to study the course of membrane reorganization during etioplast-to-chloroplast differentiation in these lines using transmission electron microscopy (TEM; Fig. 2 *B* and *C* and *SI Appendix*, Figs. S5–S7). We observed that the disassembly of PLBs proceeded faster in *curt1abcd* than in Col-0 and was completed within the first 6 h after induction of de-etiolation (Fig. 2*B* and *SI Appendix*, Fig. S5). In contrast, PLB structures persisted for longer in oe*CURT1A* than in Ler-0 and were still visible after 24 h of illumination (Fig. 2*C* and *SI Appendix*, Fig. S6). The PT structures were also altered in oe*CURT1A*, exhibiting either discontinuous or tubular patterns visible in TEM cross-sections (from 0 to 9 h into the de-etiolation process) (*SI Appendix*, Fig. S6). Given the intrinsic membrane-bending capacity of CURT1A (and other CurT proteins) previously observed in in vitro experiments (21, 24), we speculate that CURT1A provokes distortions within PTs that lead to discontinuity of PTs within the focal plane. However, regular grana-like pairing of folded single PT membranes also occurs in oe*CURT1A*, as shown in *SI Appendix*, Fig. S7. In addition, etioplasts of *curt1abcd* mutants showed loosely packed vesicle-like structures around the PLBs (Fig. 2*B*). These vesicle-like structures were in close proximity to the stroma-exposed PLB domains (*SI Appendix*, Fig. S8 *A* and *B*). We did not observe these structures in *curt1abcd* or in any other genotype between 3 and 24 h into the de-etiolation process. Only after 48 h of illumination, we again observed accumulation of vesicles in *curt1abcd* (Fig. 2). Higher-resolution images showed that similar to the observations in etiolated tissue, the vesicle-like structures were in close proximity to the membranes and exclusively in nonappressed areas near the grana stacks (*SI Appendix*, Fig. S8 *C* and *D*).

Immunogold electron microscopy confirmed the enrichment of CURT1A within the PLBs and PTs of Col-0, Ler-0, and oe*CURT1A* in etiolated samples (*SI Appendix*, Fig. S9*A*) and in

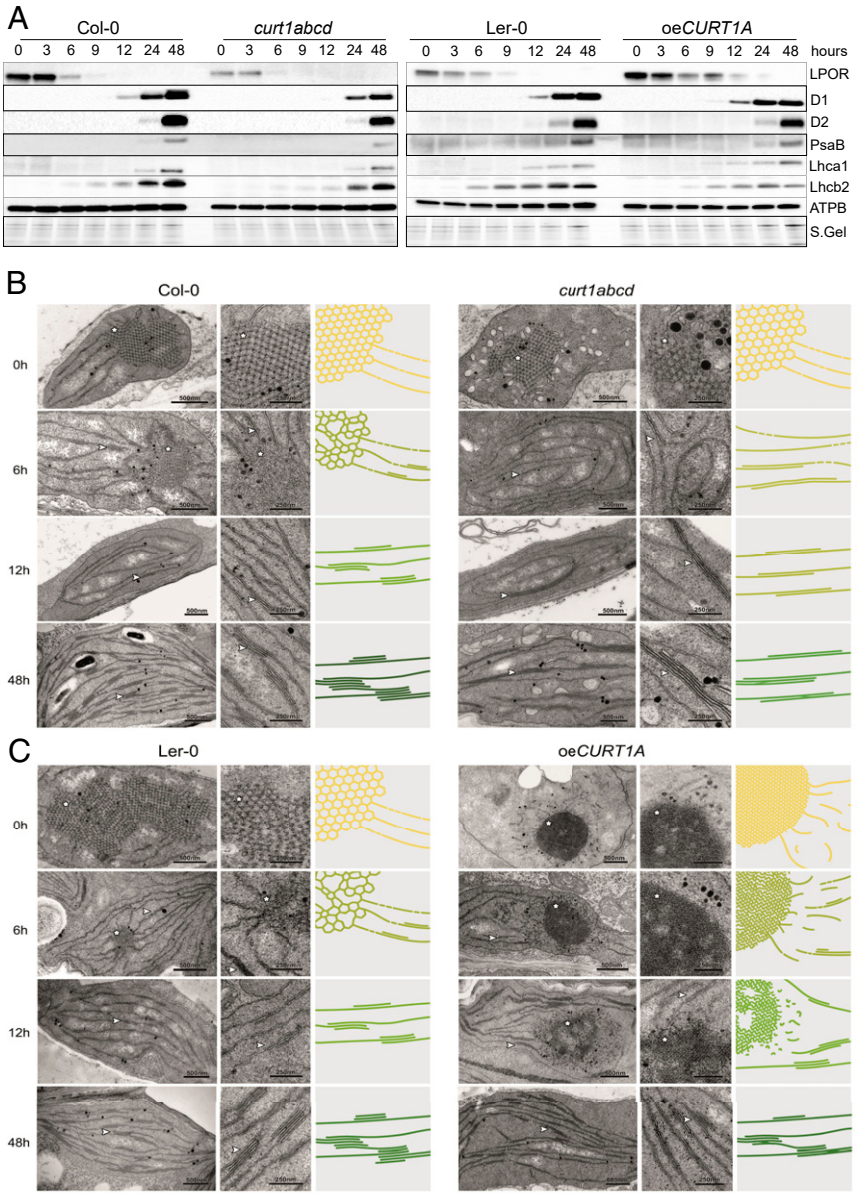

Fig. 2. Protein profiles are affected by structural changes in PLBs and PTs in *curt1abcd* and oe*CURT1A*. (*A*) Protein profiles of 7-d-old seedlings were determined at 0 to 48 h of de-etiolation in the *curt1abcd* mutant and the corresponding WT Col-0 (*Left*) and in the oe*CURT1A* line and its respective WT control (Ler-0; *Right*). At each time point, 10-μg aliquots of total protein were fractionated by sodium dodecyl sulfate polyacrylamide gel electrophoresis (SDS-PAGE) and subjected to immunoblot analysis ($n = 3$). (*B* and *C*) Transmission electron micrographs of chloroplasts from (*B*) Col-0 and *curt1abcd* and (*C*) Ler-0 and oe*CURT1A* after 0, 6, 12, and 48 h of illumination (*Left* and *Middle*). Schematic depictions of the respective membrane morphologies (scaled by average PLB size and compactness, grana sizes, and grana thylakoid interconnectivity) are presented (*Right*). Note that for clarity, the PLB network is magnified threefold relative to the size of grana stacks (membrane thickness is fixed), and the color schemes depict relative levels of chlorophyll accumulating in the respective genotypes. Stars and arrowheads indicate PLBs and stacked membranes, respectively. (Scale bars, 500 nm [*Left*, TEM] and 250 nm [*Middle*, TEM magnification].)

etio-chloroplasts after 12 h of illumination (*SI Appendix*, Fig. S9*B*). This observation was confirmed by immunogold detection of the c-Myc-tagged version of CURT1A expressed in oe*CURT1A* (*SI Appendix*, Fig. S9 *A* and *B*). Notably, a marked enrichment of gold nanoparticles, indicative of the presence of CURT1A, was observed in PLBs of etio-chloroplasts of oe*CURT1A* after 12 h of illumination (*SI Appendix*, Fig. S8*B*).

PLBs Acquire an Unusual Morphology upon Excessive Accumulation of CURT1A. The pronounced and contrasting differences in PLB morphology between *curt1abcd* and oe*CURT1A* prompted us to characterize the PLB structure in more detail. We noted that the cross-sectional areas of the PLB unit cells in *curt1abcd* and oe*CURT1A* differed significantly from those of the respective WTs. The mean cross-sectional PLB unit cell area in *curt1abcd* was 1.3 times higher than in Col-0 (2,654 ± 105 nm^2 and 2,060 ± 215 nm^2, respectively), whereas *oeCURT1A* showed a 15-fold reduction in comparison to Ler-0 (183 ± 13 nm^2 and 2,672 ± 145 nm^2, respectively; Fig. 3*A*). In addition, we observed a higher PLB tubule diameter in *curt1abcd* (27.09 ± 3.03 nm) in comparison to Col-0 (21.85 ± 2.5 nm; Fig. 3*B*). In contrast, the tubule diameter was strongly reduced in oe*CURT1A* (17.42 ± 2.19 nm)

in comparison to the corresponding WT Ler-0 (29.72 ± 2.36 nm; Fig. 3*B*). To obtain more detailed information on PLB geometry, we analyzed etiolated cotyledons from Col-0, Ler-0, *curt1abcd*, and oe*CURT1A* seedlings by ET (Fig. 3*C*). Using a surface projection, image recognition method that enables matching of TEM images with computed projections of bicontinuous phases (25), we found that the PLB lattice in all examined genotypes adopts a cubic membrane organization of a diamond type (D-type; Fig. 3 *D* and *E*). Significant differences between TEM images of the oe*CURT1A* PLB network and those of the other examined plants are therefore mostly related to a decreased size of the PLB unit cell in this genotype (Fig. 3 *A* and *E*—unit cell marked in purple). Moreover, we analyzed the spatial parameters of the PLB network inner-to-outer volume ratio (V_i/V_o) and the area-to-volume ratio (A/V_i) parameters (26) based on reconstructed three-dimensional (3D) tomograms. We observed an increase in the V_i/V_o of the paracrystalline structure in oe*CURT1A* plants, indicating significant changes in the balance between inner and outer aqueous channels of the PLB (Fig. 3*C*). In addition, we observed a higher A/V_i in oe*CURT1A*, which indicates increased PLB compactness calculated from actual 3D visualization of the periodic surface. The higher the A/V_i value, the more compact are PLBs (i.e., more membranes are present in a given volume; Fig. 3*C*). We also assessed the PLB morphology of a *curt1a* mutant in the Ler-0 background, an ecotype which is characterized by a larger unit cell size than Col-0 (*SI Appendix*, Fig. S10 *A–F*). This

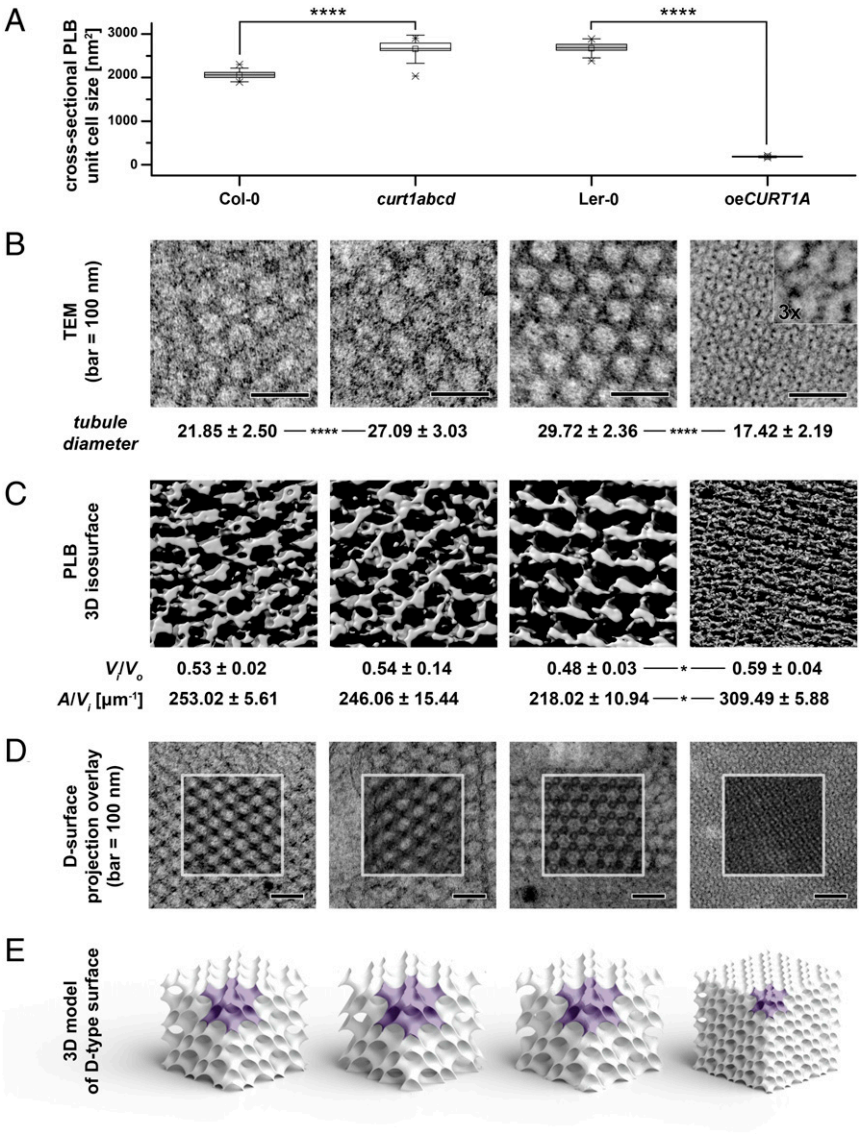

Fig. 3. Packing and morphology of PLBs is altered by either lack or excess of CURT1 proteins. (*A*) Mean cross-sectional areas of the unit cells of paracrystalline PLB lattices calculated from transmission electron micrographs of Col-0, *curt1abcd*, Ler-0, and oe*CURT1A*. Error bars represent the SD. Col-0 was compared with *curt1abcd* and Ler-0 with oe*CURT1A* by two-way ANOVA with Bonferroni posttest; ****$P < 0.001$. (*B*) Sections obtained from Col-0, *curt1abcd*, Ler-0, and oe*CURT1A* and examined by TEM. The tubule diameters for Col-0, *curt1abcd*, Ler-0, and oe*CURT1A* are indicated below each image. (*C*) 3D isosurface reconstructions of TEM sections from Col-0, *curt1abcd*, Ler-0, and oe*CURT1A*. The spatial PLB parameters of inner-to-outer volume ratio (Vi/Vo), and area-to-inner volume ratio (A/Vi) were calculated based on PLB 3D isosurface reconstructions of electron tomographs of PLBs from Col-0, *curt1abcd*, Ler-0, and oe*CURT1A*. (*D*) Electron micrographs of PLB lattices and computed projections of D-type surfaces obtained with the SPIRE tool; regions marked with white squares show a superposition of computed projections and TEM images using multiply blend mode. (*E*) 3D spatial models of cubic D-type PLB grids generated based on parameters obtained with the SPIRE tool. Single PLB unit cells are marked with purple, and all models are shown to scale, representing actual differences between unit cell sizes and volume proportion of the PLB network in particular genotypes ($n = 3$ for tomograms and reconstructions).

analysis revealed significant disturbances of PLB formation in etioplasts of *curt1a* plants. PLBs were fragmented and exhibited local irregularities, indicating the unstable nature of these structures at the level of both whole PLBs and particular unit cells (*SI Appendix*, Fig. S10 *A–C*). Measurements of the cross-sectional PLB unit cell size for recognized D-type surfaces showed a significant increase in the values registered for *curt1a* compared to Ler-0 (*SI Appendix*, Fig. S10 *D–F*). Moreover, we observed faster LPOR degradation and increased accumulation of Lhcb2 and AtpB in *curt1a* compared to Ler-0 (*SI Appendix*, Fig. S10*G*), which reflected in delayed greening (*SI Appendix*, Fig. S10*H*), similar to the observation made between Col-0 and *curt1abcd*.

Despite these differences in PLB structure, all four tested genotypes (Col-0, Ler-0, *curt1abcd*, and oe*CURT1A*) exhibited grana stacking after 6 h of de-etiolation (*SI Appendix*, Fig. S5). Next, we measured grana diameter and grana height after 6, 12, 24, and 48 h of illumination (*SI Appendix*, Fig. S10). In agreement with previous studies (5), grana height and grana diameter increased over time in both Col-0 and Ler-0. From the onset of grana formation, grana diameters in *curt1abcd* exceeded those in Col-0, without displaying much plasticity during thylakoid maturation (*SI Appendix*, Fig. S11*A*). In contrast, oe*CURT1A* showed a reduction in grana diameter compared to Ler-0, which was exacerbated upon illumination (*SI Appendix*, Fig. S11*B*). No striking differences in grana height were observed between Col-0 and *curt1abcd* or in Ler-0 versus oe*CURT1A*. To investigate whether the alterations in grana diameter observed in *curt1abcd* and oe*CURT1A* correlate with changes in 3D grana structure, we used ET to explore the changes in thylakoid spatial morphology after 48 h of de-etiolation (Fig. 4). Col-0, Ler-0, and oe*CURT1A* displayed a similar spatial distribution of thylakoid membrane structures (5), with well-defined grana core and margin areas, while *curt1abcd* showed perforated grana with numerous instances of local splitting of grana. Additionally, *curt1abcd* lacks the typical extended stroma thylakoids that normally connect neighboring grana stacks and exhibits accumulation of several vesicle-like structures. After 48 h, WT grana exhibited small membrane stacks with local membrane staggering, indicating the initiation of the typical helical arrangement of grana (27) (Fig. 4).

Onset of Photosynthesis and PS Complex Assembly Are Markedly Delayed in *curt1abcd*. To analyze the influence of both altered thylakoid biogenesis and protein accumulation on the onset of photosynthetic activity, we measured light induction curves with the aid of pulse amplitude modulation (PAM) fluorometry. In accordance with previous reports (13), a fluorescence signal was registered in etiolated seedlings of all genotypes, and its intensity decreased during the first 6 h of illumination. In seedlings collected after 6 h of de-etiolation, a chlorophyll fluorescence peak originating from PSII (black arrows, *SI Appendix*, Fig. S11) was observed in Col-0, Ler-0, and oe*CURT1A* but appeared only after 9 h of illumination in *curt1abcd*. Compared to Col-0, etiolated *curt1abcd* seedlings generally displayed a reduced maximum quantum yield of photosystem II (Fv/Fm) over the course of de-etiolation, whereas oe*CURT1A* and Ler-0 showed similar Fv/Fm values (Fig. 5*A*). The initial decline in Fv/Fm values can be ascribed to Pchlide reduction upon illumination and the concomitant accumulation of various intermediates in chlorophyll biosynthesis, while its subsequent rise reflects the increase in chlorophyll levels (Fig. 5*A*) and the accompanying onset of PSII assembly after 6 h of illumination. After 9 h of illumination, PSII activity had increased more rapidly in Col-0, Ler-0, and oe*CURT1A* than in *curt1abcd*. Indeed, PSII function remained limited in *curt1abcd* throughout the stages of chloroplast biogenesis examined (Fig. 5*A*).

To address the differences in PSII functionality observed in *curt1abcd*, the assembly of photosystem I and II complexes was analyzed using 77 K fluorescence spectroscopy (Fig. 5 *B* and *C* and *SI Appendix*, Fig. S12). Fluorescence emission spectra of etiolated cotyledons showed two distinct maxima at 632 and 654 nm, which derive from free Pchlide and photoactive Pchlide:LPOR:NADPH complexes, respectively (12). In both Col-0 and Ler-0, the 654-nm peak was higher than the 632-nm peak, while the opposite was observed for *curt1abcd* and oe*CURT1A* (Fig. 5*B*). After 3 h of illumination, these peaks had transitioned into a sharp peak at 679 nm, corresponding to chlorophyll that is not yet associated with photosystems (13), and a second broad peak between 716 and 728 nm in all genotypes examined (Fig. 5*B*). The two peaks at 723 nm and 716 nm indicate the appearance of PSI core complexes in Col-0 and *curt1abcd*, respectively (Fig. 5*B*). Both Col-0 and Ler-0 exhibited the PSI core complex peak at 723 nm (Fig. 5*B*). However, oe*CURT1A* exhibited a peak at 728 nm that was previously attributed to assembled PSI-LHCI (13, 28), which is consistent with the earlier appearance of the PSI antenna protein Lhca1 as observed by immunoblotting in oe*CURT1A* (Fig. 2*A*).

All genotypes displayed similar and progressive formation of PSII-LHCII complexes, represented by a peak at 680 nm, which first emerged after 6 h of illumination (Fig. 5*B*). However, in *curt1abcd*, formation of PSI-LHCI was noticeably delayed, as indicated by the retarded appearance of the shift in peak maximum from 716 to 728 nm. Despite the differences observed in *curt1abcd* and oe*CURT1A* at early stages of de-etiolation, chlorophyll emission spectra after 48 h of illumination were qualitatively similar to those observed in mature plants (*SI Appendix*, Fig. S12*A*). The difference spectrum *curt1abcd* versus Col-0 at 48 h featured a higher 697-nm peak on excitation at 470 nm than at 412 nm, which indicates that the higher contribution of the PSII-related peak in this genotype is mainly due to an increased LHCII antenna content (probably in aggregated states) rather than the typical PSII supercomplexes (Fig. 5*C* and *SI Appendix*, Fig. S13*B*). These differences in fluorescence are also consistent with the differences in the accumulation of PSII core proteins and LHCII proteins between *curt1abcd* and Col-0 detected by immunoblotting (Figs. 2*A* and 5 *B* and *C*). Finally, we explored the possible effects of CURT1A-mediated changes on the dynamics of Pchlide to Chlide conversion using either flash illumination of the samples for 1 ms (FL) or 15 s of dim-light exposition (LL) (*SI Appendix*, Fig. S14). Such illumination conditions affected mainly the ∼654-nm photoactive Pchlide peak. A lack of this band was seen in flash-illuminated samples, and instead, a new 685-nm peak corresponding to Chlide bound to LPOR-NADP+ was observed. Dim-light illumination (15 s) resulted in reduced intensity of the ∼654-nm band and the presence of a broad 675-nm peak representing Chlide after the Shibata shift. In both illumination conditions, the spectra of *curt1abcd* seedlings were very similar to the WT, with a lower contribution of the ∼654-nm peak in 15 s LL and the 685-nm peak after 1 ms of FL in the *curt1abcd* mutant (*SI Appendix*, Fig. S14 *A*). These results are consistent with the lower levels of LPOR protein in *curt1abcd* compared to Col-0 (Fig. 2*A*). We did not observe any delay in photoactive Pchlide conversion in oe*CURT1A* in any of the applied light settings in comparison to Ler-0 seedlings (*SI Appendix*, Fig. S13*B*). Moreover, an increase in the 675-/685-nm peaks was visible in oe*CURT1A* compared to Ler-0 (*SI Appendix*, Fig. S14*B*), in line with the higher LPOR levels detected in this genotype (Fig. 3*A*). Taken together, our results demonstrate that CURT1 proteins play a role in the concerted assembly of photosynthetic complexes and the timing of the onset of photosynthesis but do not contribute to LPOR oligomerization.

Discussion

For decades, the formation of PLBs, their disassembly upon illumination, and the latter's contribution to autotrophic growth have been the subject of many studies in model plants, including rice, wheat, bean, pea, tobacco, and *A. thaliana* (2, 3, 29, 30).

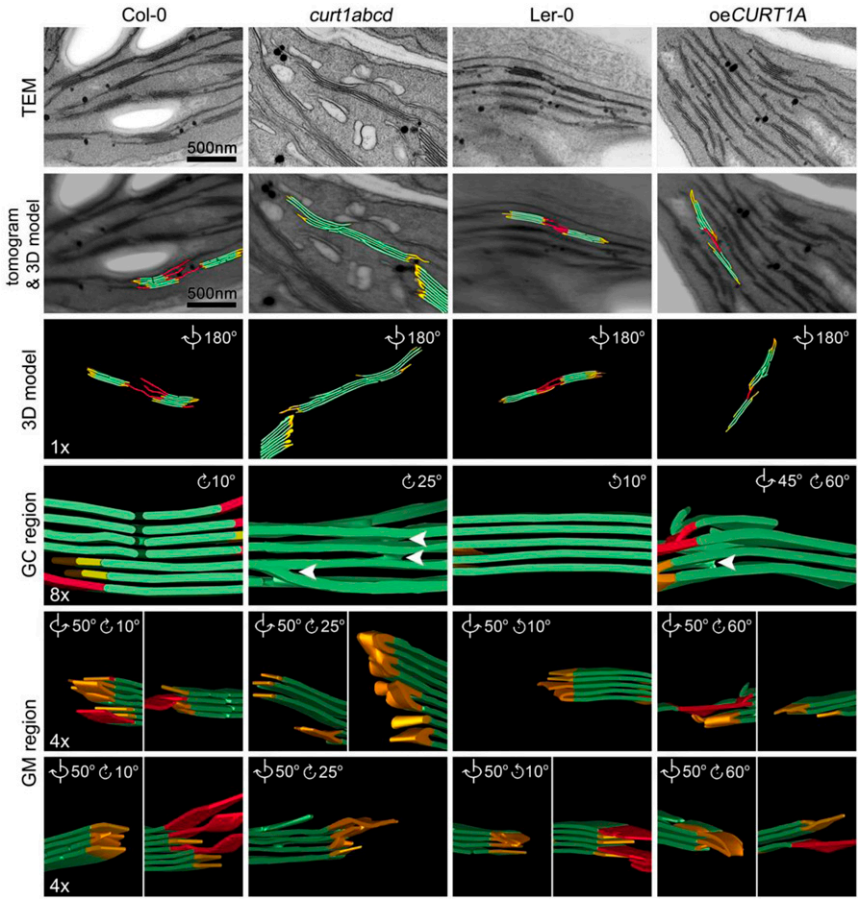

Fig. 4. Electron tomographic reconstruction of thylakoid membranes after 48 h of illumination electron tomographic reconstructions of thylakoid membranes in Col-0 (*Left*), *curt1abcd* (*Middle Left*), Ler-0 (*Middle Right*), and oe*CURT1A* (*Right*) lines based on TEM sections. Each column shows (from *Top* to *Bottom*) the central section of the TEM stack (TEM), a surface model (colored in red for stroma thylakoids, green for grana thylakoids, and yellow for grana margins) superimposed on the reconstructed tomogram, a surface visualization shown in reversed view (3D model), and magnified and rotated views of the grana core (GC region) and grana margins (GM region). White arrowheads indicate the dichotomous splitting of the membranes observed in *curt1abcd* and oe*CURT1A* sections. Scale bars and magnifications are the same for all genotypes in each row.

These studies have suggested that the morphology and geometry of PLBs depend on their lipid composition, protein content, and pigment accumulation. Loss of either of the galactolipid biosynthesis-related genes *MGD1* and *DGD1*, which are required for the synthesis of monogalactosyldiacylglycerol (MGDG) and digalactosyldiacylglycerol (DGDG), respectively, has severe effects on the size and the arrangement of the paracrystalline membranes of PLBs and on PT protrusion, suggesting that the morphology and biogenesis of PLBs depends on the MGDG/DGDG ratio (31). Similarly, accumulation of the LPOR protein has been proposed as a key requirement for PLB formation (32). The absence of PLB structures from the *porA* mutant negatively affects chloroplast differentiation and plant development, indicating that PORA plays a role in PLB organization and chloroplast differentiation, and its content is also influenced by the MGDG/DGDG ratio (33, 34). Indeed, overexpression of PORA rescues the abnormal PLB morphology observed in the *cop1* mutant (in which photomorphogenesis is disrupted) (35), which supports a role for LPOR in PLB formation. Additionally, the carotenoid-related mutant *ccr2* lacks PLBs but expresses WT levels of LPOR and has normal Pchlide contents (36). The finding that the loss of PLBs is rescued by additional mutations in the ζ-carotene isomerase (37) argues for a role for carotenoids in PLB biogenesis but not in disassembly upon illumination. It has been proposed that CURT1 proteins could contribute to thylakoid maturation during proplastid-to-chloroplast differentiation (38). Our results reported here demonstrate that CURT1 proteins accumulate in membrane fractions of etioplasts and influence the architecture and packing density of PLBs as well as the arrangement of PTs in etiolated seedlings. Although lower levels of the Pchlide:LPOR:NADPH complex were observed in both etiolated *curt1abcd* and oe*CURT1A* seedlings (compared to the WT), in all genotypes, the complex had disappeared after 3 h of illumination. Nevertheless, the accumulation of LPOR, and its subsequent degradation upon light exposure is influenced by the CURT1-mediated alterations in PLB morphology, as reflected in the lower abundance and slightly faster degradation of LPOR in *curt1abcd*, and its greater abundance and delayed degradation in oe*CURT1A* (Fig. 6). Our results strongly suggest that the Pchlide:LPOR:NADPH complex is not the only essential component for PLB maintenance, as suggested previously, since it becomes undetectable after 3 h of illumination in all genotypes studied here. Further, we cannot reject the notion that LPOR, either by itself or in association with other proteins/pigments, or the previously proposed VIPP1 (39) contributes to the maintenance of PLBs (32, 40). Although the lower content of LPOR in *curt1abcd* is directly related to the reduced accumulation of the corresponding transcript, we speculate that the size of the PLB unit cell defines the content of LPOR and/or its accessibility to lipid/membrane-remodeling proteins (e.g., proteases responsible for LPOR degradation). In this scenario, the higher LPOR content observed in oe*CURT1A*, even after 24 h of illumination, could be

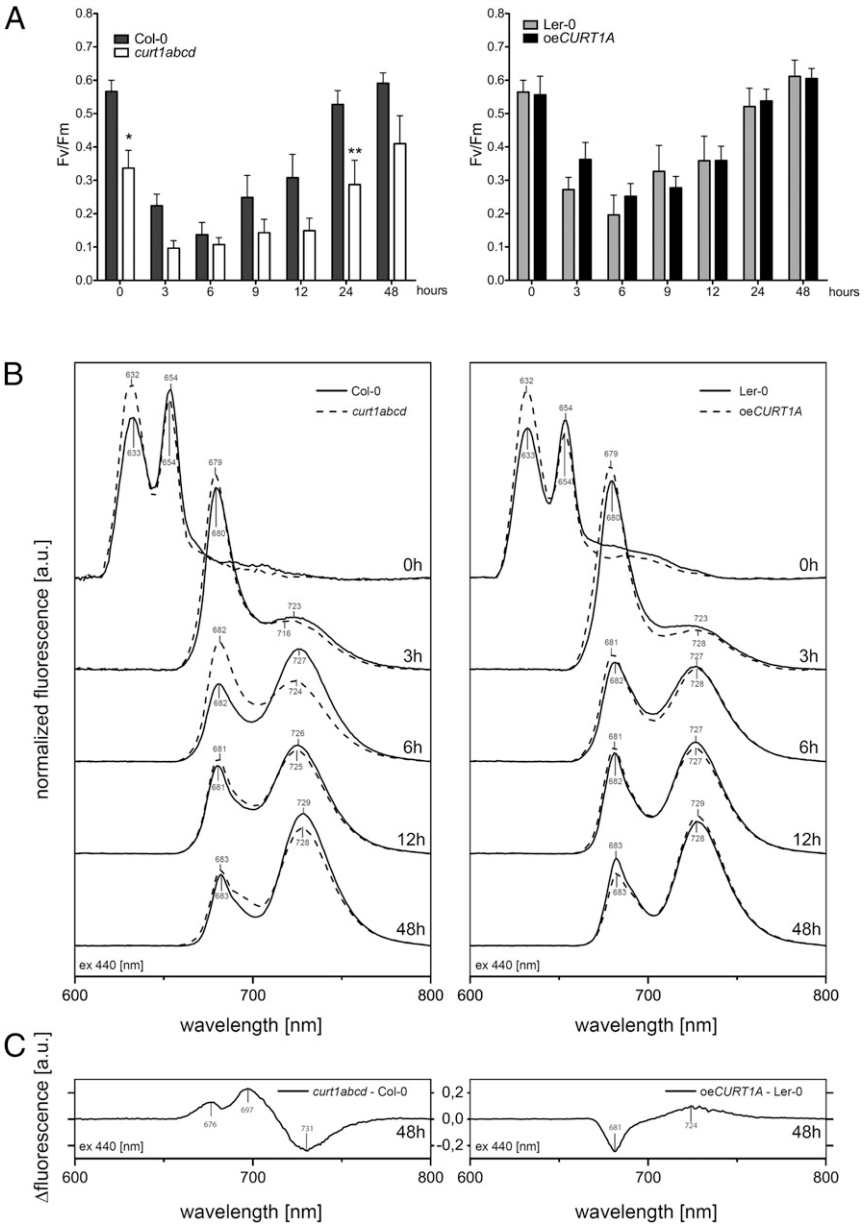

Fig. 5. The onset of photosynthesis and the assembly of photosynthetic complexes is markedly delayed in *curt1abcd*. (*A*) Comparisons of Fv/Fm values derived from PAM measurements of etiolated Col-0 and *curt1abcd* (*Left*) and Ler-0 and oe*CURT1A* (*Right*) seedlings after 0, 3, 6, 9, 12, 24, and 48 h of illumination ($n = 5$; two-way ANOVA, with Bonferroni posttest; $^{*}P < 0.05$; $^{**}P < 0.01$). (*B*) Low-temperature (77 K), steady-state fluorescence curves for Col-0 (solid line) and *curt1abcd* (dashed line) (*Left*) and Ler-0 (solid line) and oe*CURT1A* (dashed line) (*Right*) at the indicated times after induction of de-etiolation. (*C*) Fluorescence difference spectra (excitation at 440 nm) for the indicated genotypes after 48 h of illumination. Spectra are representative of three independent measurements.

related to the supercondensed nature of PLBs in this mutant line. In addition, we speculate that CURT1 proteins might be involved in the tubular-to-lamellar transition and may contribute to establishing the optimal MGDG/DGDG ratio required for the regulation of Pchlide:LPOR:NADPH complex activity (41) and for the effective redistribution of membranes from disassembled PLBs into thylakoid membranes. However, this hypothesis remains to be tested.

We note the presence of abundant swollen vesicles exclusively in etiolated tissue in *curt1abcd*, in the context of PLB synthesis, and after 48 h of de-etiolation, when de novo membrane synthesis is already active. Vesicles are not observed between 3 and 24 h, during which time formation of the lamellar membrane system mainly proceeds by the direct transformation of already synthesized PLB membranes that signals their structural transition from tubular to lamellar (5). No delay in the initiation of grana formation was observed in *curt1abcd*, since the tubular-to-lamellar transformation at the onset of de-etiolation is fed by membrane material derived from the PLBs and does not require extensive transport from the envelope. Therefore, lack of CURT1 proteins presumably results in de novo synthesis of the thylakoid network through formation of swollen vesicles rather than direct connection of the envelope with the internal plastid membrane network. This hypothesis is supported by the lack of contact sites between thylakoids and plasma membrane in the *Synechocystis CurT* mutant (24) and argues for a role of CURT1 proteins in the transport of lipids and proteins from the inner envelope to the thylakoid membranes, as previously suggested (38).

As has been shown in earlier studies, we observed an increase in the accumulation of photosynthesis-related proteins during de-etiolation. We also confirmed the presence of Cytb_6f, ATPase, and

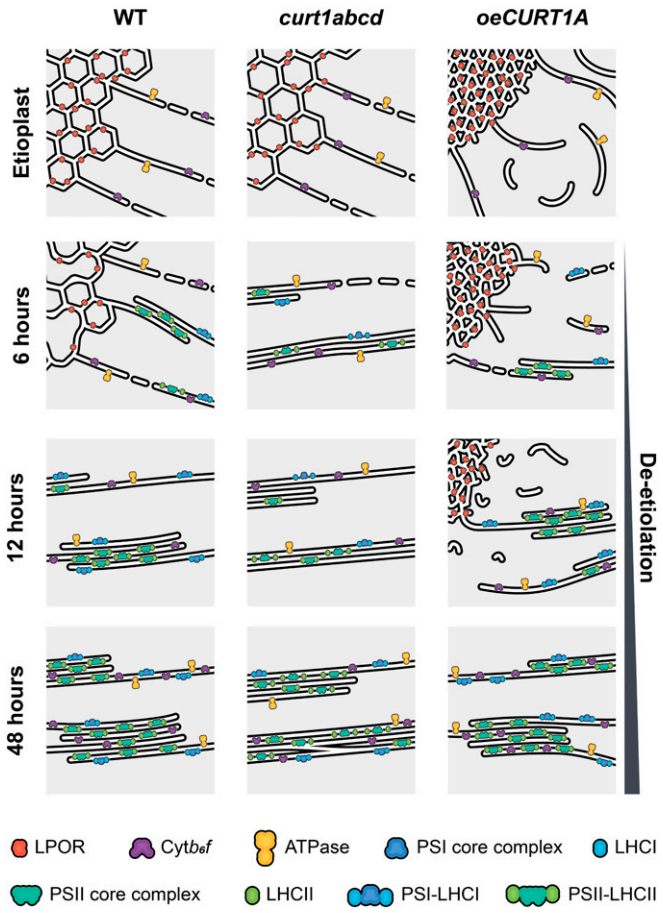

Fig. 6. Proposed model for changes in membrane morphology and the distribution of proteins across membranes observed during de-etiolation in WT, *curt1abcd*, and oe*CURT1A* seedlings. The model summarizes the correlations between structure, protein accumulation, and assembly of photosynthetic complexes observed in WT (*Left*), *curt1abcd* (*Middle*), and oe*CURT1A* (*Right*) etioplasts before and after 6, 12, and 48 h of illumination.

Rubisco-related proteins in the etioplast (1, 9). Interestingly, the accumulation of PSI- and PSII-related proteins is delayed in *curt1abcd*, which is consistent with the delay in chlorophyll accumulation. In contrast, the protein profiles of oe*CURT1A* and Ler-0 were similar overall, except for Lhca1, Lhcb2, and CP43. Despite the lower content of Lhcb2 and higher content of Lhca1 proteins observed in oe*CURT1A*, we did not observe any major changes in chlorophyll accumulation relative to Ler-0 within the first 24 h of de-etiolation. Rates of accumulation of mRNA and protein contents are poorly correlated during chloroplast development (42, 43), as is prominently exemplified by the LHC-related genes. Both *Lhca1* and *Lhcb2* transcripts exhibited two expression peaks at 3 and 24 h, corresponding to the two distinct developmental phases previously reported (3, 44). However, the magnitude of transcript accumulation was lower in *curt1abcd* compared to Col-0. Since *Lhcb2* has been used as a marker for retrograde signaling (45), we presume that communication between chloroplasts and the nucleus is, to some extent, affected in *curt1abcd*. One of the most-studied regulatory feedback mechanisms in retrograde signaling is the tetrapyrrole pathway, which involves Pchilide-dependent anchoring of glutamyl-transefer ribonucleic acid reductase (GluTR) to the thylakoid membranes by protein FLUORESCENT (FLU) (46, 47). We speculate that the morphological changes in the thylakoid membranes might negatively affect the interaction between LPOR and FLU, resulting in faster accumulation of active GluTR in oe*CURT1A*, which might explain the slightly higher chlorophyll content after 48 h of illumination, compared to Ler-0. In contrast, *curt1abcd* showed reduced chlorophyll content, most likely due to decreased photoactive LPOR rather than alterations in FLU–Pchilide interaction. In agreement with this hypothesis, our results show that the Pchlide to Chlide conversion is not affected in *curt1abcd* or oe*CURT1A*, suggesting that the morphological changes in PLBs do not affect LPOR oligomerization. However, we did observe differences in Pchlide and Chlide profiles in oe*CURT1A*, which might be explained by a higher LPOR content and possibly a higher content of active GluTR.

The stacking of grana has been attributed to the accumulation of LHCII and PSII complexes and develops from lateral extension (increase in granum diameter) to vertical grana stacking, providing a protective milieu for the assembly of PSII (5, 48–50). Our results show that all studied genotypes display membrane-stacking after 6 h of light exposure, suggesting that CURT1 proteins are not required for the initiation of grana formation during de-etiolation (Fig. 6). However, the *curt1abcd* mutant is impaired in the regulation of grana diameter throughout de-etiolation, which points to a role for CURT1 proteins in the shaping of grana or, more specifically, the establishment of defined grana margins within stroma thylakoids, as proposed before (38). In contrast, the process of vertical grana stacking itself proceeds in a similar fashion in all the genotypes after 6 h of illumination and is correlated with the onset of and subsequent increase in photosynthetic activity (as determined by PAM fluorometry) and the formation of PSII and PSI complexes, as detected by 77-K spectroscopy (Fig. 6). However, ET of thylakoid membranes derived from Col-0, *curt1abcd*, Ler-0, and oe*CURT1A* after 48 h of illumination supports the assumption that thylakoid maturation has not reached completion in any of these genotypes by that point, as their thylakoids did not show the spatial organization of grana typical of mature leaves (21). Moreover, in *curt1abcd* and oe*CURT1A* in particular, thylakoid membranes continue to show splits/discontinuities within the grana stacks (Fig. 6). Only *curt1abcd* showed fewer stroma thylakoids and multiple grana membrane perforations that might facilitate the movement of elements from stroma to grana, in a manner similar to that proposed for cyanobacteria (51). Though oe*CURT1A* showed structural differences from WT, the overall composition of its major photosynthetic complexes was unchanged, whereas the changes observed in *curt1abcd* were correlated with abnormalities in the assembly of photosynthetic complexes and the attachment of LHCII to PSII. However, we cannot disregard the possibility that the aberrant LHCII-PSII association might reflect the action of non-photochemical quenching mechanisms that are active at early stages of de-etiolation (48, 52).

Although the mechanisms behind CURT1-mediated regulation of thylakoid biogenesis are still not fully understood, our results demonstrate that CURT1 proteins are present in etioplasts and localize to PLB and PT membranes. Loss of CURT1 proteins results in a looser packing of the PLB paracrystalline lattice and leads to faster disassembly of PLBs, delayed protein accumulation, reduced chlorophyll synthesis, and accumulation of LHCII that does not become associated with PSII, all of which ultimately results in delayed onset of photosynthesis (Fig. 6). In contrast, overaccumulation of CURT1A primarily induces denser packing of PLBs, which correlates with increased LPOR content, but has no negative effects on protein or chlorophyll accumulation, complex assembly, or photosynthetic capacity after 48 h of de-etiolation (Fig. 6). Further studies using both *curt1abcd* and oe*CURT1A* will help us to gain a deeper understanding of the structural roles of PLBs and PTs, and their impact on MGDG/DGDG lipid ratios, carotenoid contents, and retrograde signaling between chloroplasts and the nucleus.

Materials and Methods

Information on plant material used, growth conditions, and experimental procedures employed in this study are detailed in *SI Appendix*. The provided methods comprise specifics on (thylakoid-) protein extraction and immunodecoration, RNA extraction and qRT-PCR, chlorophyll quantification, PAM fluorometry, and low-temperature (77 K) steady-state fluorescence measurements. Further, details about imaging techniques used (i.e., TEM, ET, and immuno-electron microscopy) are supplied.

Data Availability. All study data are included in the article and/or *SI Appendix* and all raw data are available upon request from the corresponding authors.

ACKNOWLEDGMENTS. M.P. acknowledges funding from the Novo Nordisk Foundation (NNF15OC0016586), the Danish Council for Independent Research (7017-00122A), and the Copenhagen Plant Science Centre, University of Copenhagen. Ł.K. acknowledges funding from the National Science Centre, Poland, under Grant No. 2019/35/D/NZ3/03904. R.B. acknowledges financial support from the Deutsche Forschungsgemeinschaft (FOR 2092; BO 1482/17-2). A.S. was the recipient of a postdoctoral fellowship from the Carlsberg Foundation. We thank the Center for Advanced Bioimaging at the University of Copenhagen for providing facilities for TEM sample preparation and microscopy and the Core Facility for Integrated Microscopy in the Panum Institute (University of Copenhagen) for assistance with immunogold labeling and microscopy.

1. E. Kanervo *et al*., Expression of protein complexes and individual proteins upon transition of etioplasts to chloroplasts in pea (*Pisum sativum*). *Plant Cell Physiol.* **49**, 396–410 (2008).
2. T. Armarego-Marriott, O. Sandoval-Ibañez, Ł. Kowalewska, Beyond the darkness: Recent lessons from etiolation and de-etiolation studies. *J. Exp. Bot.* **71**, 1215–1225 (2020).
3. T. Armarego-Marriott *et al*., Highly resolved systems biology to dissect the etioplast-to-chloroplast transition in tobacco leaves. *Plant Physiol.* **180**, 654–681 (2019).
4. G. A. Armstrong, S. Runge, G. Frick, U. Sperling, K. Apel, Identification of NADPH: protochlorophyllide oxidoreductases A and B: A branched pathway for light-dependent chlorophyll biosynthesis in *Arabidopsis thaliana*. *Plant Physiol.* **108**, 1505–1517 (1995).
5. Ł. Kowalewska, R. Mazur, S. Suski, M. Garstka, A. Mostowska, Three-dimensional visualization of the tubular-lamellar transformation of the internal plastid membrane network during runner bean chloroplast biogenesis. *Plant Cell* **28**, 875–891 (2016).
6. L. A. Blomqvist, M. Ryberg, C. Sundqvist, Proteomic analysis of highly purified prolamellar bodies reveals their significance in chloroplast development. *Photosynth. Res.* **96**, 37–50 (2008).
7. A. von Zychlinski *et al*., Proteome analysis of the rice etioplast: Metabolic and regulatory networks and novel protein functions. *Mol. Cell. Proteomics* **4**, 1072–1084 (2005).
8. M. Ryberg, C. Sundqvist, Spectral forms of protochlorophyllide in prolamellar bodies and prothylakoids fractionated from wheat etioplasts. *Physiol. Plant.* **56**, 133–138 (1982).
9. T. Kleffmann *et al*., Proteome dynamics during plastid differentiation in rice. *Plant Physiol.* **143**, 912–923 (2007).
10. C. Sundqvist, C. Dahlin, With chlorophyll pigments from prolamellar bodies to light-harvesting complexes. *Physiol. Plant.* **100**, 748–759 (1997).
11. Y. Lu, Identification and roles of photosystem II assembly, stability, and repair factors in Arabidopsis. *Front. Plant Sci.* **7**, 168 (2016).
12. F. Franck *et al*., Regulation of etioplast pigment-protein complexes, inner membrane architecture, and protochlorophyllide a chemical heterogeneity by light-dependent NADPH:protochlorophyllide oxidoreductases A and B. *Plant Physiol.* **124**, 1678–1696 (2000).
13. L. Rudowska, K. Gieczewska, R. Mazur, M. Garstka, A. Mostowska, Chloroplast biogenesis–Correlation between structure and function. *Biochim. Biophys. Acta* **1817**, 1380–1387 (2012).
14. S. Hartings *et al*., The DnaJ-like zinc-finger protein HCF222 is required for thylakoid membrane biogenesis in plants. *Plant Physiol.* **174**, 1807–1824 (2017).
15. N. Zagari *et al*., SNOWY COTYLEDON 2 promotes chloroplast development and has a role in leaf variegation in both *Lotus japonicus* and *Arabidopsis thaliana*. *Mol. Plant* **10**, 721–734 (2017).
16. K. Kobayashi, S. Fujii, M. Sato, K. Toyooka, H. Wada, Specific role of phosphatidylglycerol and functional overlaps with other thylakoid lipids in Arabidopsis chloroplast biogenesis. *Plant Cell Rep.* **34**, 631–642 (2015).
17. Kobayashi K, *et al*. Role of galactolipid biosynthesis in coordinated development of photosynthetic complexes and thylakoid membranes during chloroplast biogenesis in Arabidopsis. *Plant J.* **73**, 250–261 (2013).
18. X. Xu *et al*., Convergence of light and chloroplast signals for de-etiolation through ABI4-HY5 and COP1. *Nat. Plants* **2**, 16066 (2016).
19. T. Sun *et al*., ORANGE represses chloroplast biogenesis in etiolated Arabidopsis cotyledons via interaction with TCP14. *Plant Cell* **31**, 2996–3014 (2019).
20. S. Fujii, N. Nagata, T. Masuda, H. Wada, K. Kobayashi, Galactolipids are essential for internal membrane transformation during etioplast-to-chloroplast differentiation. *Plant Cell Physiol.* **60**, 1224–1238 (2019).
21. U. Armbruster *et al*., Arabidopsis CURVATURE THYLAKOID1 proteins modify thylakoid architecture by inducing membrane curvature. *Plant Cell* **25**, 2661–2678 (2013).
22. M. Pribil, *et al*., CURT1-mediated thylakoid plasticity is required for fine-tuning photosynthesis and plant fitness. *Plant Physiol.* (2018).
23. R. Hohner *et al*., Plastocyanin is the long-range electron carrier between photosystem II and photosystem I in plants. *Proc. Natl. Acad. Sci. U.S.A.* **117**, 15354–15362 (2020).
24. S. Heinz, *et al*. Thylakoid membrane architecture in synechocystis depends on CurT, a homolog of the granal CURVATURE THYLAKOID1 proteins. *Plant Cell* **28**, 2238–2260 (2016).
25. T. M. Hain, *et al*. SPIRE, surface projection image recognition environment for bicontinuous phases: Application for plastid cubic membranes. *bioRxiv* [Preprint] (2021). https://doi.org/10.1101/2021.04.28.441812 (Accessed 29 April 2021).
26. M. Bykowski *et al*., Spatial nano-morphology of the prolamellar body in etiolated *Arabidopsis thaliana* plants with disturbed pigment and polyprenol composition. *Front. Cell Dev. Biol.* **8**, 586628 (2020).
27. Y. Bussi *et al*., Fundamental helical geometry consolidates the plant photosynthetic membrane. *Proc. Natl. Acad. Sci. U.S.A.* **116**, 22366–22375 (2019).
28. A. Andreeva, K. Stoitchkova, M. Busheva, E. Apostolova, Changes in the energy distribution between chlorophyll-protein complexes of thylakoid membranes from pea mutants with modified pigment content. I. Changes due to the modified pigment content. *J. Photochem. Photobiol. B* **70**, 153–162 (2003).
29. A. Seluzicki, Y. Burko, J. Chory, Dancing in the dark: Darkness as a signal in plants. *Plant Cell Environ.* **40**, 2487–2501 (2017).
30. S. Fujii, H. Wada, K. Kobayashi, Role of galactolipids in plastid differentiation before and after light exposure. *Plants* **8**, 357 (2019).
31. S. Fujii, K. Kobayashi, N. Nagata, T. Masuda, H. Wada, Digalactosyldiacylglycerol is essential for organization of the membrane structure in etioplasts. *Plant Physiol.* **177**, 1487–1497 (2018).
32. D. Floris, W. Kühlbrandt, Molecular landscape of etioplast inner membranes in higher plants. *Nat. Plants* **7**, 514–523 (2021).
33. T. Paddock, D. Lima, M. E. Mason, K. Apel, G. A. Armstrong, Arabidopsis light-dependent protochlorophyllide oxidoreductase A (PORA) is essential for normal plant growth and development. *Plant Mol. Biol.* **78**, 447–460 (2012).
34. S. Fujii, K. Kobayashi, N. Nagata, T. Masuda, H. Wada, Monogalactosyldiacylglycerol facilitates synthesis of photoactive protochlorophyllide in etioplasts. *Plant Physiol.* **174**, 2183–2198 (2017).
35. U. Sperling *et al*., Etioplast differentiation in arabidopsis: Both PORA and PORB restore the prolamellar body and photoactive protochlorophyllide-F655 to the cop1 photomorphogenic mutant. *Plant Cell* **10**, 283–296 (1998).
36. H. Park, S. S. Kreunen, A. J. Cuttriss, D. DellaPenna, B. J. Pogson, Identification of the carotenoid isomerase provides insight into carotenoid biosynthesis, prolamellar body formation, and photomorphogenesis. *Plant Cell* **14**, 321–332 (2002).
37. C. I. Cazzonelli *et al*., A *cis*-carotene derived apocarotenoid regulates etioplast and chloroplast development. *eLife* **9**, e45310 (2020).
38. Z. Liang *et al*., Thylakoid-bound polysomes and a dynamin-related protein, FZL, mediate critical stages of the linear chloroplast biogenesis program in greening Arabidopsis cotyledons. *Plant Cell* **30**, 1476–1495 (2018).
39. J. Theis *et al*., VIPP1 rods engulf membranes containing phosphatidylinositol phosphates. *Sci. Rep.* **9**, 8725 (2019).
40. W. Wietrzynski, B. D. Engel, Chlorophyll biogenesis sees the light. *Nat. Plants* **7**, 380–381 (2021).
41. M. Gabruk, B. Mysliwa-Kurdziel, J. Kruk, MGDG, PG and SQDG regulate the activity of light-dependent protochlorophyllide oxidoreductase. *Biochem. J.* **474**, 1307–1320 (2017).
42. R. Zoschke, R. Bock, Chloroplast translation: Structural and functional organization, operational control, and regulation. *Plant Cell* **30**, 745–770 (2018).
43. P. Chotewutmontri, A. Barkan, Dynamics of chloroplast translation during chloroplast differentiation in maize. *PLoS Genet.* **12**, e1006106 (2016).
44. C. Dubreuil *et al*., Establishment of photosynthesis is controlled by two distinct regulatory phases. *Plant Physiol.* **176**, 1199–1214 (2017).
45. A. C. McCormac, M.J. Terry, The nuclear genes Lhcb and HEMA1 are differentially sensitive to plastid signals and suggest distinct roles for the GUN1 and GUN5 plastid-signalling pathways during de-etiolation. *Plant J.* **40**, 672–685 (2004).
46. Y. Fang *et al*., The Arabidopsis glutamyl-tRNA reductase (GluTR) forms a ternary complex with FLU and GluTR-binding protein. *Sci. Rep.* **6**, 19756 (2016).
47. Z. Hou, Y. Yang, B. Hedtke, B. Grimm, Fluorescence in blue light (FLU) is involved in inactivation and localization of glutamyl-tRNA reductase during light exposure. *Plant J.* **97**, 517–529 (2019).
48. D. Shevela *et al*., 'Birth defects' of photosystem II make it highly susceptible to photodamage during chloroplast biogenesis. *Physiol. Plant.* **166**, 165–180 (2019).
49. R. Kouřil, J. P. Dekker, E. J. Boekema, Supramolecular organization of photosystem II in green plants. *Biochim. Biophys. Acta* **1817**, 2–12 (2012).
50. P. Albanese, S. Tamara, G. Saracco, R. A. Scheltema, C. Pagliano, How paired PSII-LHCII supercomplexes mediate the stacking of plant thylakoid membranes unveiled by structural mass-spectrometry. *Nat. Commun.* **11**, 1361 (2020).
51. R. Nevo *et al*., Thylakoid membrane perforations and connectivity enable intracellular traffic in cyanobacteria. *EMBO J.* **26**, 1467–1473 (2007).
52. J. Sacharz, V. Giovagnetti, P. Ungerer, G. Mastroianni, A. V. Ruban, The xanthophyll cycle affects reversible interactions between PsbS and light-harvesting complex II to control non-photochemical quenching. *Nat. Plants* **3**, 16225 (2017).